Z. NOWAK*,#, M. NOWAK*, R.B. PĘCHERSKI*, M. POTOCZEK**, R.E. ŚLIWA**

MECHANICAL PROPERTIES OF THE CERAMIC OPEN-CELL FOAMS OF VARIABLE CELL SIZES

WŁASNOŚCI MECHANICZNE PIANEK CERAMICZNYCH O OTWARTYCH KOMÓRKACH I RÓŻNEJ POROWATOŚCI

The mechanical properties and numerical model of ceramic alumina open-cell foam, which is produced by the chemical method of gelcasting with different cell sizes (porosities) are presented. Geometric characteristics of real foam samples were estimated from tomographic and scanning electron microscopy images. Using this information, numerical foam model was proposed. A good agreement between the numerical model and the results elaborated from microtomography was obtained. To simulate the deformation processes the finite element program ABAQUS was used. The main goal of this computation was to obtain macroscopic force as a function of applied vertical displacement in compression test.

As a result of numerical simulation of compression test of alumina foam for different values of porosity, the Young modulus and the strength of such foams were estimated.

Keywords: mechanical properties of foams, alumina open-cell foam, Young modulus, strength of alumina foams

W pracy określono własności mechaniczne i przedstawiono model numeryczny ceramicznej pianki korundowej (α- Al$_2$O$_3$) o komórkach otwartych i różnej porowatości, otrzymanej metodą żelowania spienionej zawiesiny (gelcasting). Metoda ta pozwala na tworzenia pianek zawierających różnej wielkości komórki a w konsekwencji na otrzymywanie pianek o różnej porowatości.

Wielkości charakteryzujące geometrię rzeczywistych pianek ustalono z wykorzystaniem tomograficznych obrazów 3D oraz obrazów z mikroskopu skaningowego. Informacje te wykorzystano przy opracowywaniu modelu numerycznego takiej pianki. Uzyskano model numeryczny o dużej zgodności symulowanej mikrostruktury z obrazami otrzymanymi z mikrotomografu. Symulacje numeryczne procesu deformacji przeprowadzono przy użyciu programu elementów skończonych ABAQUS. Z symulacji numerycznych otrzymano zmianę wielkości siły w funkcji przemieszczenia górnej powierzchni. Określono również zmianę modułu Younga oraz wytrzymałości na ściskanie pianek korundowych w funkcji porowatości.

1. Introduction

The subject of our study is open-cell alumina foam. These foams have a complex microstructure consisting of interconnected randomly packed cells that evolve during the foaming process. The microstructure of such a foam defines unique mechanical, thermal, acoustical and functional properties (e.g., see Gibson and Ashby [6]). The alumina foams distinctive features are following: high porosity, high mechanical stiffness and good thermal shock resistance. In recent years there has been published many papers which deal with the estimation of mechanical behaviour of foams. In these models e.g. Nieh at al. [17], Zhou et al. [18] and Michailidis et al. [19] the microstructure of porous foam is the main point of research, while the influence of damage or local microcracking is omitted. It is very important to find the effective mechanical properties of foams as a function of porosity. The presented study is focused on determination of Young modulus and compression strength of alumina foams based on the novel approach relating the microtomography analysis with the constitutive modelling of the foam behaviour. The paraboloid yield condition is applied in the formulation of the quasi-brittle material models.

The finite element models of alumina open-cell foams are developed and elastic properties and compressive strength were predicted and compared with experimental results. The first family of foams models is based on the mircotomograthy pictures showing the structure of cells. The second family of the computer generated models are based on impacted bubbles simulation resulting in random cells structure. The simulation of the deformation process of the specimen under compression was also performed.

The calculated compressive response starts with a linearly elastic regime. At higher stress levels, inelastic deformation, produced by the multiscale mechanisms of microcracking

* INSTITUTE OF FUNDAMENTAL TECHNOLOGICAL RESEARCH, POLISH ACADEMY OF SCIENCES, 02-106 WARSZAWA, PAWINSKIEGO 5B, POLAND

** RZESZÓW UNIVERSITY OF TECHNOLOGY, 35-959 RZESZÓW, AL. POWSTANCÓW WARSZAWY 12, POLAND

Coressponding author: znowak@ippt.pan.pl

and damage evolution in the foam skeleton, causes a gradual material degradation and reduction of its stiffness.

Many ceramic materials and composites reveal the strength differential effect. In such a case the plasticity theory based on Huber-Mises-Hencky yield condition to describe inelastic behaviour of foams is not appropriate. The proper yield condition for brittle ceramic materials is related with paraboloid yield surface, (Burzyński [10, 11], Vadillo et al. [13], Frąś et al. [12], Pęcherski et al. [14]). The identification of the paraboloid yield surface requires two independent tests: tension and compression.

2. Microstructure and morphology of alumina foams

Ceramic open-cell foam, which is produced by the chemical method of gelcasting (Potoczek [2], Ortega et al. [4, 5]) for 90% porosity is presented in Fig.1.

Fig. 1. Cylindrical sample of alumina 90 % porosity foam produced by the chemical method of gelcasting; the diameter amounts 8.0 mm and the height 17.0 mm

The X-ray computed tomography was performed to characterize the foam microstructure including cell size as well as cell and windows distribution. Earlier applications of the results of tomography analysis for computational modelling of foams were presented e.g. in Michilidis et al. [9]. The distribution of ligaments cross sectional area, as described earlier in Jang et. al. [15], was also analysed. As can be seen in the foam image in Fig. 2, the cells are open in each direction of the alumina foam sample.
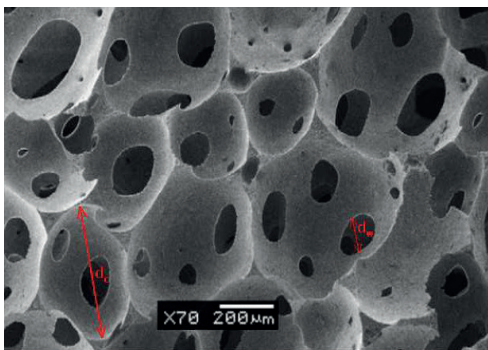

Fig. 2. Optical microscopy image of structure of alumina 90 % porosity foam with presentation of dimension of window and cell diameters, Potoczek [3]

In Fig 3a and 3b the tomographic images of 86% porous foam are presented. Equivalent porosity in 2D and in 3D was observed. Cell diameter varies in the range from 0.05 to 1.0 mm. Windows diameter equals about 1/3 of cell diameter. In Fig. 4 the histograms of cell diameter d_c , and windows diameter d_w , of real structure of alumina 90 % porosity foam obtained from tomographic microscopy images are presented.
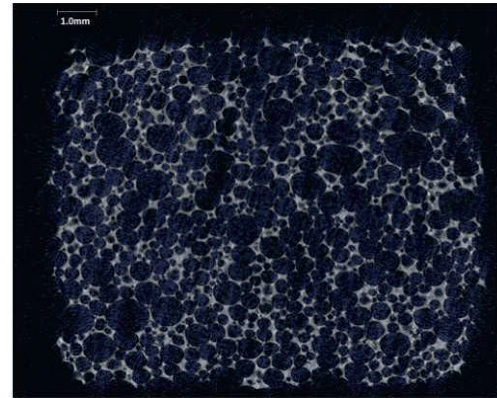
(a)
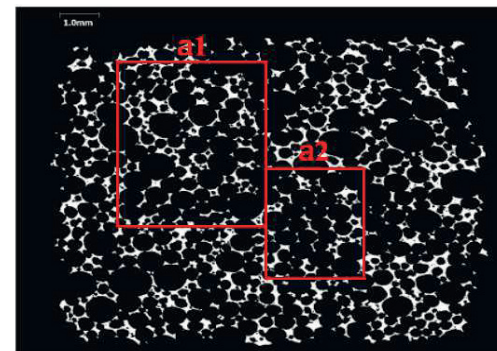
(b)

Fig. 3. (a) The raw tomographic image of alumina foam, (b) The same image with applied threshold value of pixel intensity to obtain the phase of alumina foam skeleton, from Nowak et al. [1]
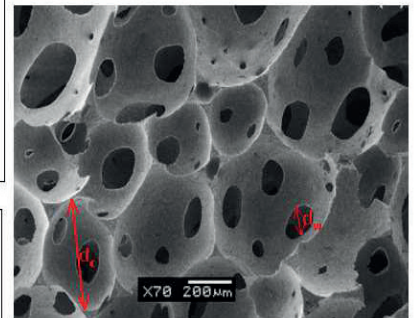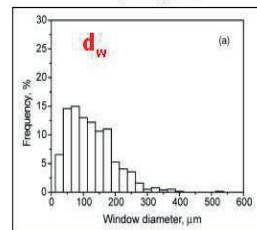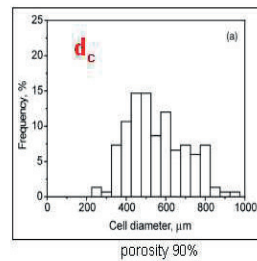

Fig. 4. The histograms of cell diameter d_c , and windows diameter d_w , of real structure of alumina 90 % porosity foam obtained from tomographic images
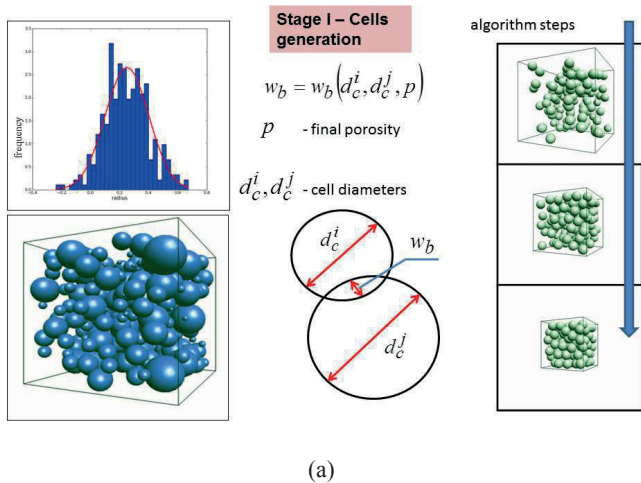
3. Numerical model of the geometry of open-cell foam structure

The Al_2O_3 foams are modelled by adopting the numerically generated structure, based on real open-cell foam shown in Fig. 1. As is seen the structure of the foam needs to be simplified. This is done by using model with random microstructure which approximates the distribution and shape of the pores of real foam.
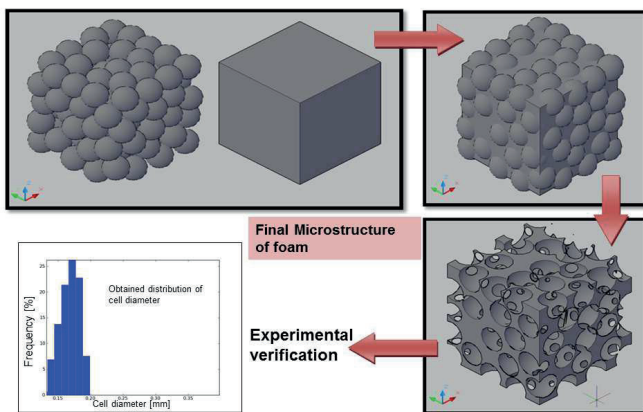
The process based on impacted bubbles simulation of random cells generates the representative foam skeleton and describes actual foam microstructures.

Geometry of ceramic foams can be generated in two steps:
- the coordinates of the centre points of the spherical bubbles and their diameters were produced by PYTHON scripts, M. Nowak [16]. The diameters of spherical bubbles and windows were estimated from microtomography and the coordinates of the centre points were determined in such a way that the bubbles have to intersect with each other, cf Fig. 5a,
- the intersecting bubbles were subtracted from the bulk volume of any shape, cf Fig. 5b.

3.1. Initial data for the generation of numerical model

The cell and windows distributions in the alumina ceramic foams show an unsymmetrical behaviour and therefore log-normal distribution may be a possible distribution to fit such data. The log-normal distribution is a continuous distribution in which the natural logarithm of a variable has the normal distribution. Thus, its probability density function, f, can be written as follows

$$f(x) = \frac{1}{x\sigma\sqrt{2\pi}} \exp\left(-\frac{(\ln(x) - \mu)^2}{2\sigma^2}\right) \qquad (1)$$

For the distribution Eq. (1) and assumed maximal and minimal values of cell diameter: r_{min} and r_{max} we can generate foams with different porosities, e.g.:
for foams of porosity 90% we assume: $r_{min} = 0.1$ [mm], $r_{max} = 0.5$ [mm] and with number of bubbles = 180
$$\sigma = 0.08 [mm], \mu = 0.256 [mm]$$
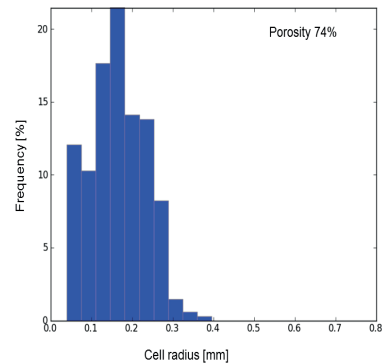for foams of porosity 86% we assume: $r_{min} = 0.1$ [mm], $r_{max} = 0.4$ [mm] with number of bubbles = 240
$$\sigma = 0.03 [mm], \mu = 0.190 [mm]$$
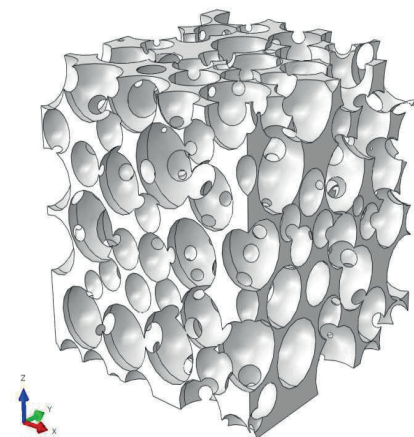for foams of porosity 74% we assume: $r_{min} = 0.02$ [mm], $r_{max} = 0.22$ [mm] and number of bubbles = 340
$$\sigma = 0.078 [mm], \mu = 0.036 [mm].$$

This makes basis for the generation of the particular foam structures illustrated in Fig. 6 and 7.

(a)

(b)

Fig. 5. The numerical foam model (a) Stage I - generation of cells, (b) Stage II-final microstructure of generated foam with the distribution of cell diameter

(a)

(a)

Fig. 6. The generated foam structure with porosity 74%
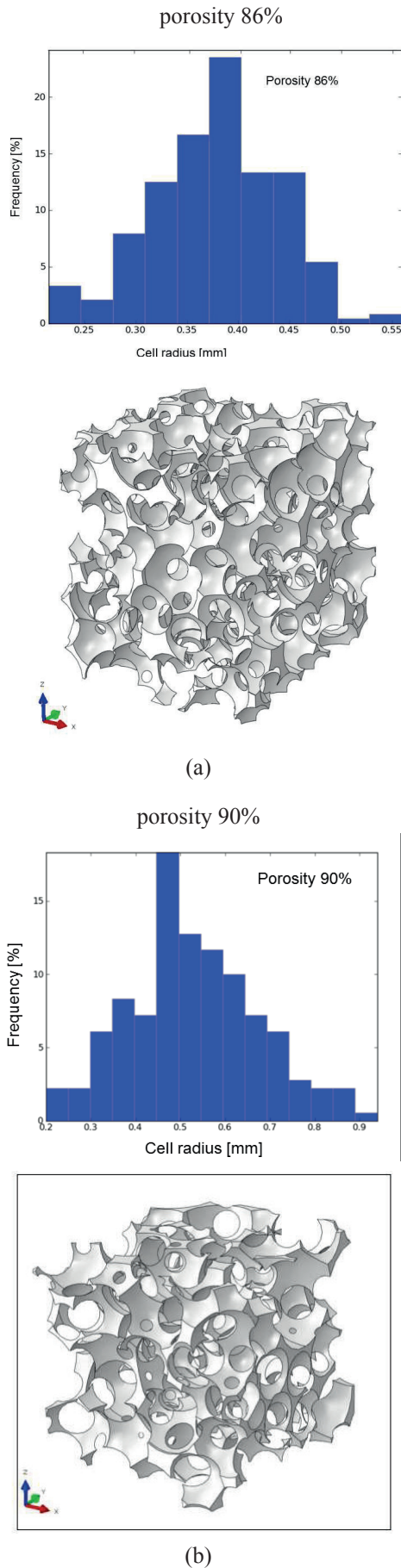
porosity 86%

porosity 90%

(a)

(b)

Fig. 7. The generated foam structures, (a) porosity 86% and (b) porosity 90%, histogram of cell size distribution (top) and general view of the foam structure (bottom)

3.2. Finite element mesh generation

The finite element discretization was derived from real foam specimen by computer tomography images using the procedures described in Nowak et al. [1]. Dimension of a finite element corresponds to the dimension of a single voxel and was equal to $16\mu m$. In all numerical calculations the cube-shaped sample of the foam with dimensions of

$400\times400\times400$ voxels was considered. This assumption gives a representative volume element (RVE) of size $4\times4\times4\ mm$. The sample was discretized for three-dimensional finite element analysis, using 4-node linear tetrahedron or 10-node quadratic tetrahedron elements. The finite element mesh generated by ABAQUS CAE is presented in Fig. 8.
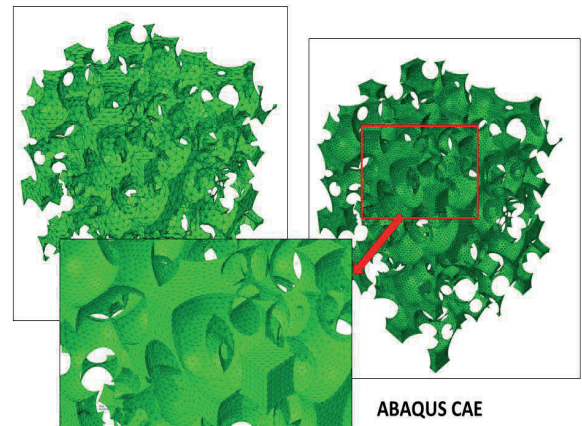

Fig. 8. The finite element mesh generated by ABAQUS CAE

4. Compression experiments

The specimens were compressed between parallel platens in a stiff electromechanical testing machine run under displacement control, see Fig. 9. The quasi-static displacement rate was $1.3\times10^{-4}s^{-1}$. The stress–displacement relations were obtained from uniaxial compression tests for the foam specimens of different porosity. The response exhibits an initial nearly linear part during which the deformation is essentially homogeneous. At the stress level of about 4.0 MPa, damage in some of the skeleton struts appears. This value can be considered as the strength of skeleton.
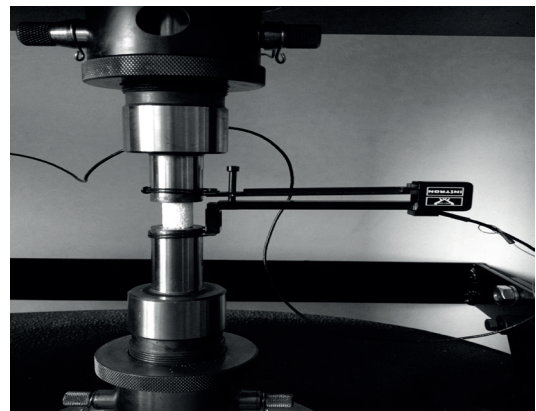

Fig. 9. The cylindrical sample of foam before mechanical test in Instron testing machine

The typical compressive nominal stress versus strain response of investigated foam is shown in Figs 10-14. A nearly linear regime terminates into a limit load. This is followed by a load plateau that extends to an average strain of about 3–6%, followed by a second stiff branch (densification). The low initial stress peak and extended load plateau are responsible for the energy absorption characteristic of such foams.
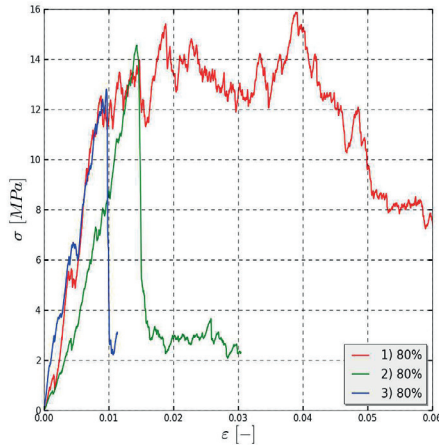

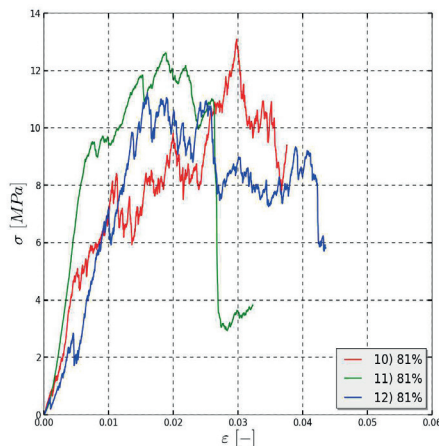Fig. 10. Nominal stress versus strain response for three 80 % porous samples

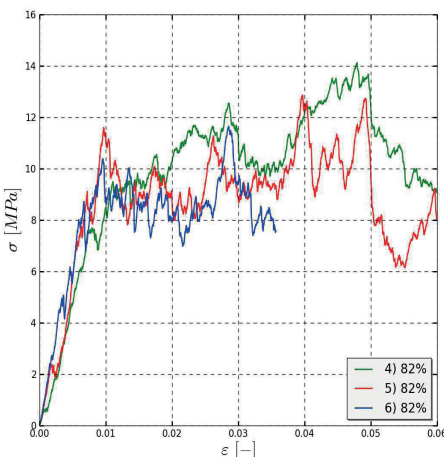Fig. 11. Nominal stress versus strain response for three 81 % porous samples

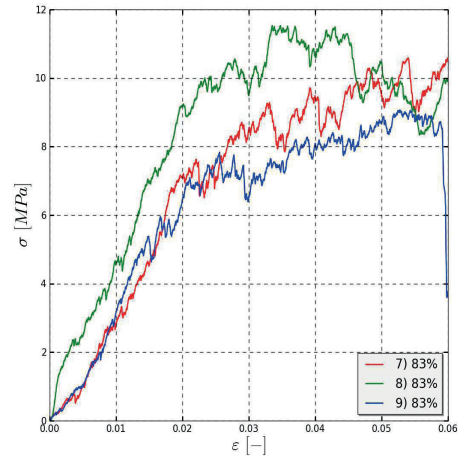Fig.12. Nominal stress versus strain response for three 82 % porous samples

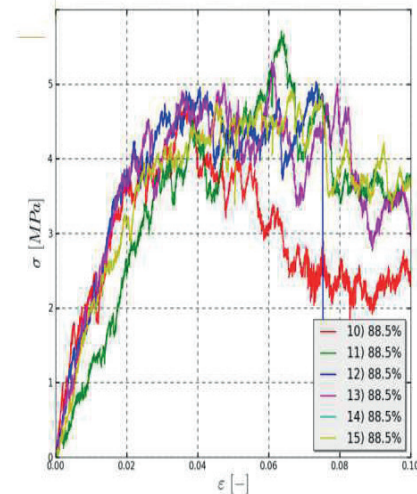Fig. 13. Nominal stress versus strain response for three 83 % porous samples

Fig. 14. Nominal stress versus strain response for six 88.5 % porosity samples

5. The quasi-brittle material model for Al₂O₃ foams

The model describing behaviour of considered ceramic foam is defined in elastic range by Hooke's law and approximated in inelastic range by the associated plasticity theory plasticity theory with assumption that yield surface is interpreted as limit surface of elastic range. The limit surface is defined by Burzyński paraboloid yield condition, Burzyński [10,11], Vadillo et al. [13], Frąś et al. [12], Pęcherski et al. [14]. The additive decomposition of small strain tensor into elastic and inelastic part is given by following equation

$$\varepsilon = \varepsilon^e + \varepsilon^{in} \tag{2}$$

The Burzyński paraboloid yield condition has following form

$$F = \frac{1}{2k}\left\{3(k-1)p + \sqrt{9(k-1)^2 p^2 + 4kq^2}\right\} - \sigma_Y^T\left(\bar{\varepsilon}^{pl}\right) = 0 \, , \, k = \frac{\sigma_Y^C}{\sigma_Y^T} \tag{3}$$

where σ_Y^C and σ_Y^T are the initial yield stress in uniaxial compression and tension test, respectively. In addition, the scalar damage parameter d is included, which modifies stress strain relation as follows

$$\boldsymbol{\sigma} = (1 - d)\boldsymbol{D^e} : (\varepsilon - \varepsilon^{in}) \qquad (4)$$

The inelastic part of strain rate is given by classical associated flow rule, where F represents limit surface given in Eq. (3)

$$\dot{\varepsilon}^{in} = \dot{\gamma}\frac{\partial F}{\partial \boldsymbol{\sigma}} \qquad (5)$$

In equation (Eq. (4) parameter d describes the damage in skeleton material and in Eq. (3) p is the hydrostatic stress while q is equivalent stress. The evolution of the damage parameter d is described by function $\eta(\varepsilon^{-in})$, where ε^{-in} is the equivalent inelastic strain, cf [16]. In the calculations the function η is assumed as the linear function of ε^{-in} with the limits of the initial value, $\varepsilon^{-in} = 0$, and final value, $\varepsilon^{-in} = \varepsilon^{-in}$:

$$d = \eta(\varepsilon^{-in}) , \eta(0) = 0, \eta(\varepsilon_k^{-in}) = 0.9 \qquad (6)$$

The system of equations describing the deformation process of the open-cell foam is solved by algorithm using the return mapping procedure. The proposed algorithm was verified by performing numerical tests with use of 4-node linear tetrahedron and 10-node quadratic tetrahedron elements in commercial FEM software ABAQUS/EXPLICIT and developed own UMAT subroutine, M. Nowak [16].

Numerical simulations of the uniaxial compression test for Al_2O_3 foams were conducted with use of ABAQUS finite element program, see also for earlier study of Kirca [8]. The ceramic foam is assumed to be isotropic. The bottom surface of the sample was fixed constrained and the top surface of the sample was moved parallel to the z-axis.

Material data for Al_2O_3 were assumed as follows:
- Young modulus - 370GPa,
- Poisson ratio – 0.22,
- the initial compression yield stress- 2400 MPa,
- the initial tensile yield stress- 105 MPa,
- density - 3.92g/cm^3.

6. The results of numerical simulations

The model outlined in Section 5 was used to predict the compressive strength in the uniaxial compression. To enforce compression state in numerical simulation, the displacement boundary condition was applied on the bottom and upper surface of the foam without friction. The bottom surface was fixed (all degrees of freedom were zero) and to the upper surface vertical displacement of magnitude of 10% of height was applied. The results of calculations are presented in Fig. 15.
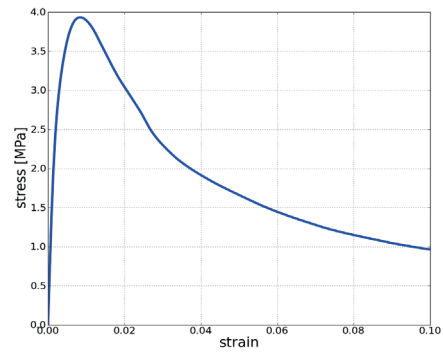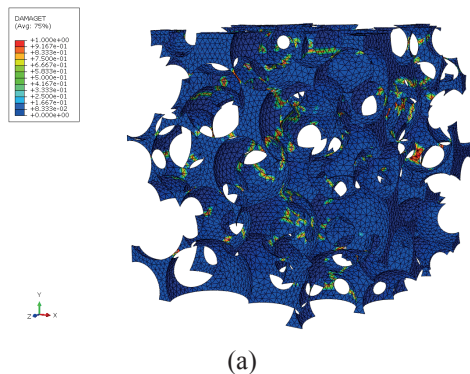
(a)

(b)

Fig. 15. (a) Contour plot of damage parameter d for foam with porosity 90% in the box 2×2×2 mm, axial displace- ment uy =0.04 mm, (b) Predicted nominal stress versus strain response

The initial part of the response is nearly linear with modulus E which is in very good agreement with measured values. The skeleton struts experience the combined axial compression and bending or tension that finally creates microcracks. Thus, the softening in macroscopic stress-strain relation is observed, cf. Fig. 15b.

Fig. 16 shows the comparison of the Young modulus from analytical (Gibson and Ashby [6], Roberts and Garboczi [7]), experimental (Potoczek [3]) and the own numerical predictions. The results show that there is a stiffening effect as the porosity increases.
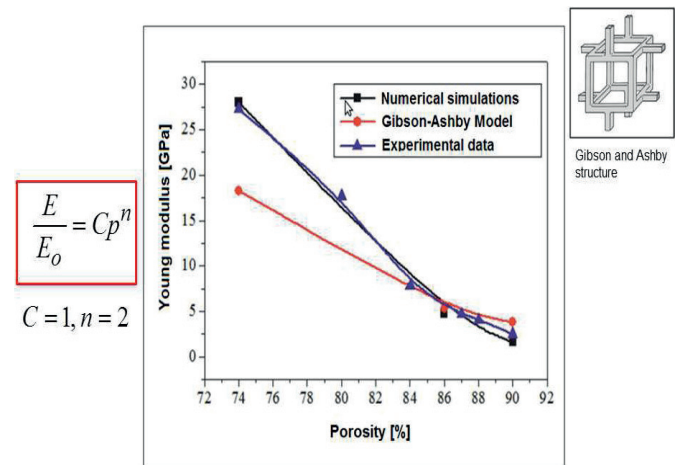
$$\frac{E}{E_o} = Cp^n$$

$$C = 1, n = 2$$

Fig. 16. The comparison of experimental data with numerical and analytical predictions

In Gibson-Ashby model E corresponds to Young modulus of porous material and E_0 corresponds to the Young modulus of dense skeleton material. The parameters C and n depend on microstructure of porous material and in the case of open-cell ceramic foams they are equal C=1 and n=2.

7. Summary and Conclusions

The microstructure of Al_2O_3 open-cell foams was characterized using X-ray computed tomography. The characterization includes measurement of cell size and windows distributions. Foams of different cell sizes corresponding to

70 - 90% porosity were considered. In numerical simulations the compressive response starts with a linear elastic range. At higher stress level inelastic deformations produce a gradual reduction of material stiffness, which eventually leads to a stress maximum that represents the strength of the material. The performance of the reconstructed models was compared to measured values of the elastic moduli and strength in the uniaxial compression test. The following observations can be made from this comparison:

- prediction of the elastic moduli obtained from the reconstructed model are in agreement with the measured values,
- prediction of the strength of the skeleton obtained from the reconstructed model is in agreement with the measured value equal to about 4.0 MPa.

REFERENCES

[1] M. Nowak, Z. Nowak, R.B. Pęcherski, M. Potoczek, R.E. Śliwa, On the reconstruction method of ceramic foam structures and the methodology of young modulus determination, Archives of Metallurgy and Materials. **58**, 1219–1222 (2013).

[2] M. Potoczek. Gelcasting of alumina foams using agarose solutions, Ceramics International. **34**, 661–667 (2008).

[3] M. Potoczek. Design of the Microsturcture of Alumina Foams (in Polish), Oficyna Wydawnicza Politechniki Rzeszowskiej, Rzeszów (2012).

[4] F.S. Ortega, P. Sepulveda, V.C. Pandolfelli, Monomer systems for the gelcasting of foams, J. Eur. Ceram. Soc. **22**, 1395–1401 (2002).

[5] F.S. Ortega, F.A.O. Valenzuela, C.H. Scuracchio, V.C. Pandolfelli, Alternative gelling agents for the gelcasting of ceramic foams, J. Eur. Ceram. Soc. **23**, 75–80 (2003).

[6] L.J. Gibson M.F. Ashby, Cellular Solids, Structure and Properties, 2nd edition, Cambridge (1999).

[7] A.P. Roberts, E.J. Garboczi, Elastic moduli of model random three-dimensional closed-cell cellular solids, Acta Mater. **49**, 189–197 (2001).

[8] M. Kirca, Computational modeling of micro-cellular carbon foams, Finite Elements in Analysis and Design. **44**, 45 – 52 (2007).

[9] N. Michailidis, F. Stergioudi, H. Omar, D.N. Tsipas , An image-based reconstruction of the 3D geometry of an Al open-cell foam and FEM modeling of the material response, Mechanics of Materials. **42**, 142–147 (2010).

[10] W. Burzyński, Selected passages from Włodzimierz Burzyński doctoral dissertation Study on Material Effort Hypotheses, Engineering Transactions. **57**, 185-215 (2009). Published orginally in Polish: W. Burzyński, Studium nad hipotezami wytężenia, Nakładem Akademii Nauk Technicznych, 1-192, Lwów 1928, also: W. Burzyński, Dzieła Wybrane, tom I, 67-258, PWN Warszawa 1982.

[11] W. Burzyn´ ski, Theoretical foundations of the hypotheses of material effort, Engineering Transactions. **56**, No. 3, 269–305 (2008) – the English translation of the paper published in Polish, Czasopismo Techniczne. **47**, 1-41 (1929). [12]

[12] T. Frąś, Z. Kowalewski, R.B. Pęcherski, A. Rusinek, Applications of Burzyński failure criteria, Part I. Isotropic materials with asymmetry of elastic range, Engng. Trans. **58** (1-2), 3-13 (2010).

[13] G. Vadillo, J. Fernandez-Saez, R.B. Pęcherski, Some applications of Burzyński yield condition in metal plasticity, Materials and Design. **32**, 628-635 (2011).

[14] R.B. Pęcherski, K. Nalepka, T. Frąś, M. Nowak, Inelastic Flow and Failure of Metallic Solids. Material Effort: Study Across Scales, in: T. Łodygowski, A. Rusinek (Eds.), Constitutive Relations under Impact Loadings, Experiments, Theoretical and Numerical Aspects, Springer, 552, 245-285, CISM, Udine (2014).

[15] W.-Y. Jang, A.M. Kraynik, S. Kyriakides, On the microstructure of open-cell foams and its effect on elastic properties, Int. J. Solids Struct. **45**, 1845–1875 (2008).

[16] M. Nowak, Analysis of deformation and failure of ceramic foam structures in application to numerical simulation of infiltration processes of alumina foam by liquid metal, PhD thesis in Polish, IPPT PAN, Warsaw (2014).

[17] T.G. Nieh, K. Higashi, J. Wadsworth, Effect of cell morphology on the compressive properties of open-cell aluminum foams, Materials Science and Engineering. **283**, 105–110 (2000).

[18] J. Zhou, P. Shrotriya, W.O. Soboyejo, Mechanisms and mechanics of compressive deformation in open-cell al foams, Mechanics of Materials. **36**, 781–797 (2004).

[19] N. Michailidis, F. Stergioudi, H. Omar, D.N. Tsipas, An image-based reconstruction of the 3D geometry of an al open-cell foam and fem modeling of the material response, Mechanics of Materials. **42**, 142–147 (2010).